***R. A. Kippersund, P. Lunde and K-E Frøysa.*** "*Hydrate deposit detection in pipes using ultrasonic guided waves", Proceedings of the 34th Scandinavian Symposium on Physical Acoustics, Geilo 30 January – 2 February, 2011.*

# Hydrate deposit detection in pipes using ultrasonic guided waves

Remi André Kippersund[1,2,3]
Per Lunde[2,1,3]
Kjell-Eivind Frøysa[1,3]

[1] Christian Michelsen Research AS, Bergen
[2] University of Bergen, Dept. of Physics and Technology, Bergen
[3] The Michelsen Centre for Industrial Measurement Science and Technology

## Abstract

*In this work, the process pipe is used as a waveguide for acoustic signals to non-invasively monitor hydrate formation as a solid deposit on the pipe wall. The guided wave modes have characteristic, frequency dependent mode shapes which contribute to how the modes interact differently with the surrounding media. Modes and methods are investigated as the deposit is considered either a semi-infinite layer, not propagating energy back to the waveguide, or a finite layer allowing for bi-layer modes to appear. Experiments have been conducted where onset of hydrate formation is detected by attenuation measurements over multiple modes. The results are compared with times of temperature increase in the pipe. It is shown feasible to obtain thickness information from bi-layer modes.*

Contact author: Kippersund, R. A., Christian Michelsen Research AS, Fantoftvegen 38, P.O. Box 6031, NO-5892 Bergen, NORWAY, email: remi.kippersund@cmr.no

## 1 Introduction

Gas hydrates are receiving considerable attention from the oil industry due to their potential hazard of plugging pipe-lines [1]. Many systems operate in the hydrate zone and rely on inhibiting chemicals and pressure/temperature calculations to avoid hydrate formation. There exist a risk of inhibitor failure or process changes, which make methods for monitoring the onset and growth of hydrate crystals highly called for.

Non-invasive techniques are of interest in this context, for operational and cost-saving reasons and to avoid interference with the flow. Ultrasonic guided waves can be used for such purposes. Techniques using ultrasonic guided waves are found in many applications. It is widely used in non destructive testing [2] and also utilized for flow process monitoring like fouling detection [3] and viscosity measurements [4], [5]. This is because different guided wave modes inherit different properties like velocity, dispersion, attenuation and sensitivity to

different kinds of waveguide impurities (like defects and loading). The many propagating modes also represent a challenge in using guided waves as the signal can become complex to analyse. A typical approach is to isolate a single mode by limiting the spatial and temporal bandwidth of the transducers [6].

In this paper, guided wave modes are studied for the purpose of non-invasively detecting onset and growth of hydrate deposits in a process pipeline. The model used for calculating dispersion curves is presented in chapter 2. The amplitude weighting between the different modes is of interest when multiple modes propagate. The theory used here for calculating this weighting, the excitability functions, for a given type of excitation is also given in this section. In chapter 3, a series of simulations are shown to give the grounds for the method chosen to solve the task. Sensitivity to a hydrate deposit in a fluid flow, and the effect of non-reflecting and reflecting layers are studied. Experiments have been conducted where onset of hydrate formation is detected by attenuation measurements over multiple modes. The experimental setup is presented in chapter 4 and results shown in chapter 5. A discussion of the results, with relation to the theory and simulation is given in chapter 6. In Chapter 7, some conclusions from this work are drawn.

# 2 Theory

## 2.1 Model for calculating dispersion curves of multilayered structures

When stress waves propagate in an isotropic solid waveguide, a theoretically infinite number of propagating modes with different phase velocities can appear. Since the guided wave modes in general are dispersive, their wavenumber-frequency relations are frequently referred to as dispersion curves. The same term is also used for quantities that can be deducted from the former, like phase velocity, group velocity, attenuation etc. The dispersion curves are important to understand the signal propagation and utilizing special properties of different modes. A program called MODEST has been implemented here for the calculation of dispersion curves in multilayered Cartesian and cylindrical systems (plates and pipes) [5]. The model is based on the global matrix method originally proposed by Knopoff [7] and the implementation closely follows that described by Pavlakovic et al. for the modelling software DISPERSE [8].

## 2.2 Groups of modes and their displacement components

There are three types of modes that can propagate along the axial direction of a pipe of cylindrical cross section. These are characterized by their displacement components: Longitudinal modes which inherit both radial and axial displacements, torsional modes with circumferential displacement components only (normal to the direction of propagation), and flexural modes which involve all radial, axial and circumferential displacement components. Only the symmetric modes (longitudinal and torsional) are considered here. These can be selected (from the flexural modes) by uniform excitation around the circumference of the pipe.

### 2.3 Analytical expression for SH modes in vacuum

In this work, special attention is paid to the shear horizontal (SH) modes, which are the plate equivalents to the torsional modes in pipes. For a single plane layer in vacuum, there exists an analytical expression for these modes. The n'th order SH mode is given by [9]

$$\frac{f^2}{c^2} - \frac{\xi_n^2}{4\pi^2} = \left(\frac{n}{2d}\right)^2, \tag{1}$$

where $f$ is the frequency, $c$ is the shear velocity of the material, $\xi_n$ is the horizontal wavenumber (wavenumber in the propagation direction) of the $n$'th mode, $n = \{0,1,2,\ldots\}$ and $d$ is the thickness of the layer. Note that the mode numbering for the SH modes starts with 0 (corresponding to T(0,1)).

### 2.4 Excitability functions for SH modes

MODEST can also be used to calculate mode shapes. That is, the displacement and stress distribution through the thickness of the layers. The mode shapes are here used, in combination with the frequency-wavenumber solution for the modes, to calculate excitability functions using the normal mode expansion technique [10].

A source on the surface is assumed extending from $-L$ to $L$ in the direction of wave propagation, $z$, with a tangential traction profile $t_y(z)$ in the direction, $y$, normal to the direction of the guided wave propagation. The amplitude, $a$, of SH mode $n$ is found by the expression

$$a_n(z) = \frac{e^{-i\xi_n z}}{4P_{nn}} \int_{-L}^{L} e^{i\xi_n \bar{z}} \tilde{v}_y(d) t_y(\bar{z}) d\bar{z} \quad \text{for } L < z, \tag{2}$$

where $P_{nn}$ is the Poynting vector of mode $n$ [10] for which the mode shapes are needed, and $v_y(d)$ is the particle velocity on the surface ($\sim$ denotes complex conjugation).

Excluding the source dependent terms in equation 2, an expression for the excitability functions is proposed,

$$\Phi_n = \frac{\tilde{v}_y(d)}{4P_{nn}} e^{-i\xi_n z}. \tag{3}$$

In section 3.3, the excitability functions are used to calculate the relative amplitudes of modes excited in single and bi-layer structures. The relative amplitudes are also investigated for attenuating modes. Note here that the normal mode expansion theory using complex reciprocity relations is strictly only valid for lossless propagation. Following the argumentation by Duquenne [11] however, the theory makes a good approximation for low loss cases. Duquenne arguments that if attenuation is sufficiently weak its effect can be neglected in the terms associated with the local Lamb wave generation. Being cumulative however, the effect should be taken into account as the waves are propagated over some distance. The validity of this approximation has not been checked here.

Rose [9] has presented the analytical expression for the excitability functions of the $SH_n$ modes for a single layer in vacuum,

$$|\Phi_n| = \frac{1}{\varepsilon_n \rho c^2} \left| \sqrt{\left(\frac{fd}{c}\right)^2 - \left(\frac{n}{2}\right)^2} \right|, \tag{4}$$

where $\rho$ is the density, $\varepsilon_0$=2 and $\varepsilon_n$=1 for $n > 0$. This expression is obtained by a different technique using spatial Fourier transforms. Eq. 5 is in section 3.3 used to check the expression for the excitability functions (eq. 4), and the calculation using MODEST results.

# 3 Simulations

The material data used in the simulations in this paper are summarized in Table 1.

**Table 1 Material properties used in simulations**

| Material | $\rho$ [kg/m³] | $c_L$ [m/s] | $c_S$ [m/s] | $\alpha^{**}$ [Np/wl] |
|---|---|---|---|---|
| Steel [12] | 7932* | 5959 | 3260 | 0 |
| $CH_4$ Hydrate [13] | 900 | 3650 | 1890 | 0.1 |
| $CH_4$ Hydrate low $c_S$ | 900 | 3650 | 189 | 0.1 |
| Ice [13] | 920 | 3900 | 1970 | 0.1 |
| Water | 1000 | 1500 | - | 0 |

*) Density should be 7923 from reference. **) Not from dataset

## 3.1 Pipe modes and influence of fluid presence

Hydrate deposits can appear both in pipes carrying liquid or gas (when there is water present). It is therefore of interest to be able to detect the deposit with minimum influence from a liquid presence. Figure 1 shows how modes are affected by filling a pipe with water. In Figure 1a the modes are plotted for a pipe in vacuum, while Figure 1b shows the modes of a pipe filled with water. Following Silk and Bainton [14], the mode numbering is *L(0,i)* for the longitudinal modes and *T(0,i)* for the torsional modes, where $i$ = {1,2,3,…} is the mode number of the respective groups and 0 stands for the circumferential order, which is nonzero only for flexural modes.

a)

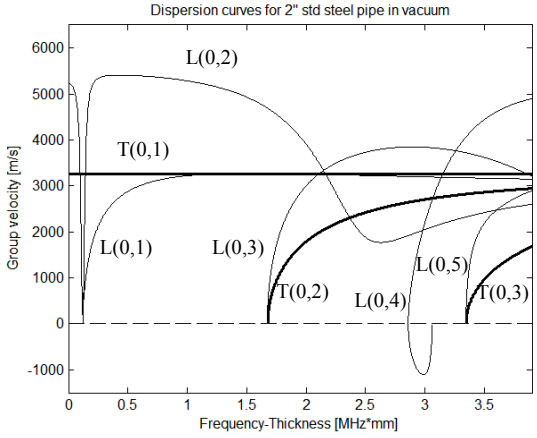


b)

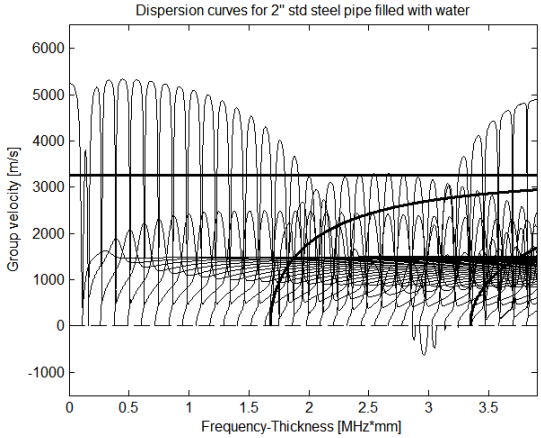


**Figure 1 : Steel pipe simulations. Group velocity dispersion curves for a 2 inch diameter pipe with wall thickness 3.91 mm. a) Pipe in vacuum, b) Pipe filled with water.**

The torsional modes, here drawn with thicker lines, are not affected by the filling of the pipe. This is due to the purely circumferential displacement components and the fact that the non-viscous fluid does not support shear stress.

The further analysis is on the torsional modes, and their sensitivity to a hydrate load. To simplify the analysis, shear horizontal (SH) modes are investigated, which may be used as an approximation for torsional modes for a large pipe diameter to wall thickness ratio [15], [16].

### 3.2 Non-reflecting loading

In some cases, the acoustic energy that enters the depositing layer never returns to the pipe wall, but gets absorbed inside the depositing layer. It could be that the layer where highly attenuating, or that the inner surface is irregular so that it scatters the signal into the fluid rather than back to the pipe. Such non-reflecting layers are here simulated as a semi-infinite layer on one side of a plate (see Figure 2).

Figure 3 shows the phase velocity and attenuation of the first four SH modes when the plate is subject to two different loading materials. The first loading material (blue lines) is $CH_4$ Hydrate as measured by Waite [13], see Table 1. The second loading material has the same properties as the former, but with one tenth of the shear velocity (denoted $CH_4$ Hydrate low $c_s$ in Table 1). The second material is included in the simulations to show the effect of changing the $c_s$ parameter.

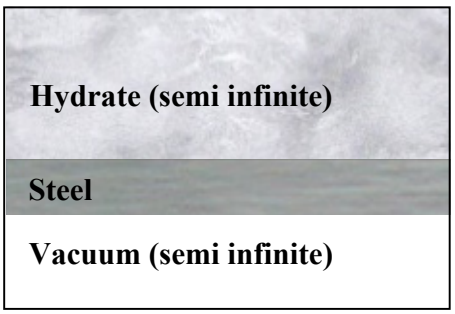


**Figure 2 Illustration of setup to simulate non-reflecting layer. Material data are given in Table 1.**

a) b)

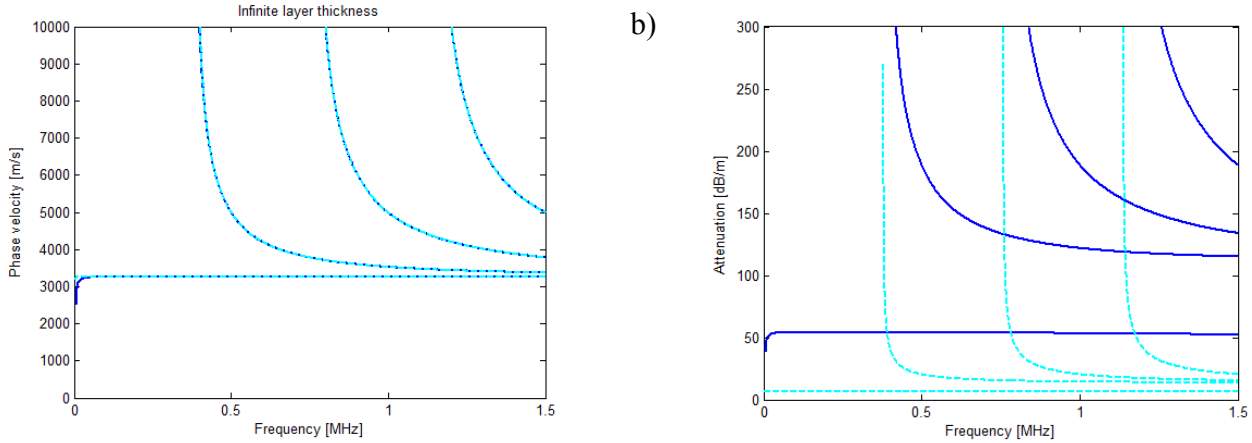


**Figure 3 Semi infinite layer of $CH_4$ Hydrate (dark blue lines) and $CH_4$ Hydrate "low $c_s$" (cyan lines) on a 4.3 mm steel plate. a) Phase velocity, b) Attenuation.**

While the phase velocity of Figure 3a is virtually unchanged, Figure 3b shows that the attenuation is sensitive to the load; the depositing layer carries energy away from the plate (the plate is assumed to be lossless). The low $c_s$ simulation shows that the attenuation is sensitive to the shear velocity of the load. In a closer study of this dependency, it has been found to be proportional to the shear impedance of the load [5]. For this type of loading, the deposit detection should therefore be based on attenuation measurements.

### 3.3 Deposit layer of finite thickness

For the case where the deposit is a uniform layer of finite thickness, the waveguide becomes one of two layers as shown in Figure 4a. To study the modes of this bi-layer waveguide, the modes of the each layer are first simulated separately. It will be shown that some key features of the bi-layer waveguide can be extracted from this analysis simplifying the interpretation of the measured results.

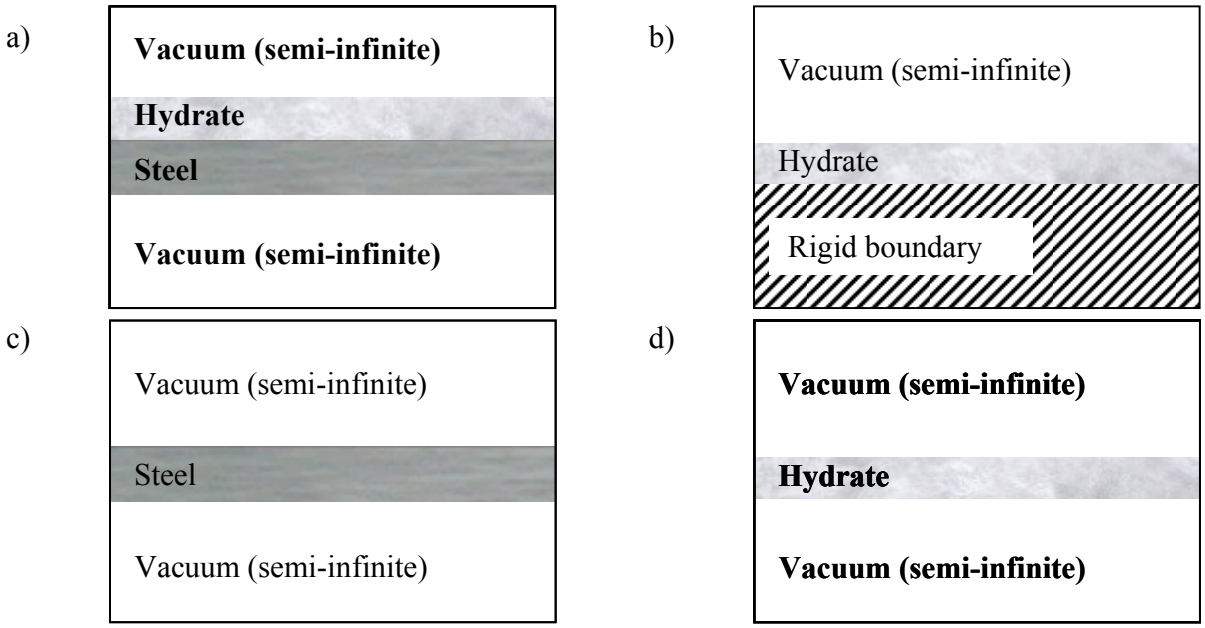


**Figure 4 Illustration of layer setups in simulations. a) Steel-Hydrate bi-layer, b) Hydrate clamped at one side, a) Steel layer free in vacuum and d) Hydrate layer free in vacuum, and.**

"Rigid points"

Figure 5 shows the SH modes of the pipe wall (solid lines) simulated as a plane layer in vacuum as in Figure 4c. The hydrate layer is calculated as a plane layer clamped at one side (dashed lines), see Figure 4b, using [17]

$$\frac{f^2}{c^2} - \frac{\xi_m^2}{4\pi^2} = \left(\frac{2m+1}{4d}\right)^2, \tag{5}$$

where the mode number for the hydrate layer is $m = \{0,1,2,\ldots\}$.

The points where these curves intersect are here called the "rigid points", which refer to the wavenumber-frequency combinations on the dispersion curves. The frequencies of these points are found by combining equation 1 and 5,

$$f_{Rigid}^2(m,n) = \frac{c_{plate}^2 c_{deposit}^2}{c_{plate}^2 - c_{deposit}^2}\left[\left(\frac{2m-1}{4d_{deposit}}\right)^2 - \left(\frac{n}{2d_{plate}}\right)^2\right], \tag{6}$$

where subscripts "plate" and "deposit" refer to the steel and the hydrate layer, respectively.

a)

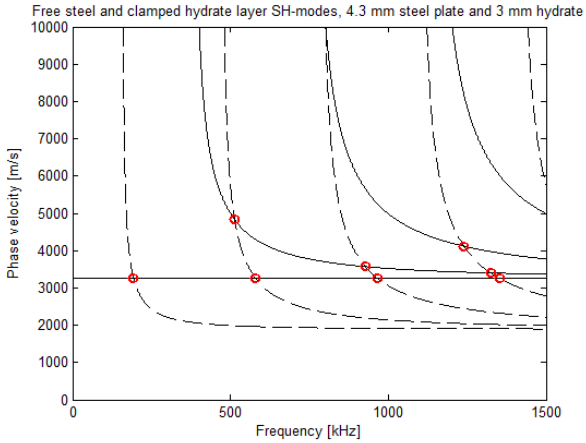


b)

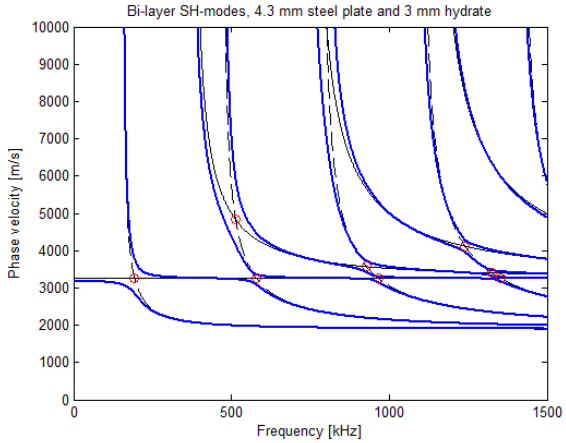


**Figure 5 a) 4.3 mm Steel plate in vacuum (solid lines) and 3 mm $CH_4$ Hydrate clamped at one side (dashed lines). Red circles indicate "Rigid points". b) Same as a. with Steel-Hydrate bi-layer overlaid (blue lines).**

In Figure 5b, with simulation setup of Figure 4a, the modes of the bi-layer waveguide are shown in blue lines overlaid the two separate layer simulations. It can be seen that the modes bend away from the rigid points and a phenomena called "mode jumping" [17] occur. Away from the rigid points, the modes approach asymptotically the modes of the two separate solutions.

a)

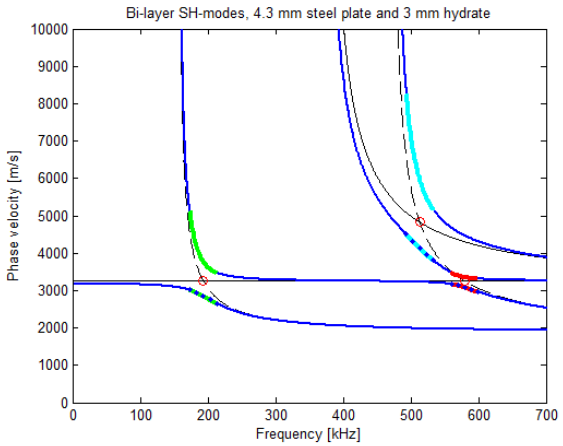


b)

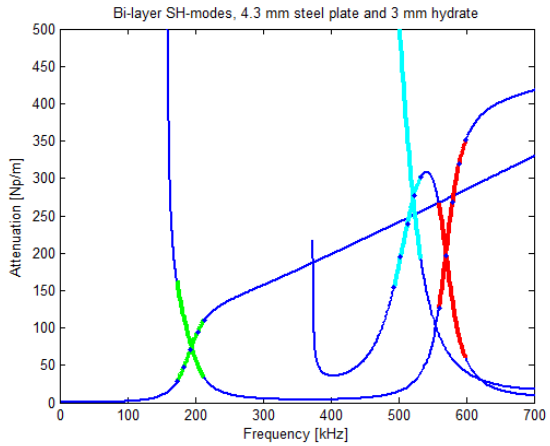


**Figure 6 a) Zoom in on Figure 5b with a 40 kHz band around the rigid points outlined with different colours. b) Attenuation of the first four bi-layer modes (same outlining colours as in a).**

Figure 6a shows a zoom in on the first four modes of Figure 5b. The frequency bands near the rigid points have been outlined with colours so they can be identified in the attenuation plot (Figure 6b).

The mode jumping can be associated with a decreasing attenuation for the modes repelling from a path of the free-clamped deposit layer; a mode propagates with least attenuation as it follows a path of the steel plate. In the transition region where one mode "takes over" the path of another, there is a frequency range of increased attenuation between them.

"Free points"

As a second case study of the finite layer, the hydrate layer is considered one in vacuum, see Figure 4d. The modes of this layer intersect the modes of the steel plate in vacuum in what is here called the "free points" on the dispersion curves, see Figure 7a. Similarly to the rigid points, the free points can be given by an analytical expression. Here using only eq. 1 for the two materials,

$$f_{Free}^2(m,n) = \frac{c_{plate}^2 c_{deposit}^2}{c_{plate}^2 - c_{deposit}^2}\left[\left(\frac{m}{2d_{deposit}}\right)^2 - \left(\frac{n}{2d_{plate}}\right)^2\right]. \quad (7)$$

It can be seen that the free points are also solutions of the bi-layer modes. These points are also marked in the attenuation plot of the bi-layer modes (Figure 7b) where it can be seen that these points are located near the attenuation minimum of their mode. This phenomenon has also been discussed by Simonetti [17].

a)

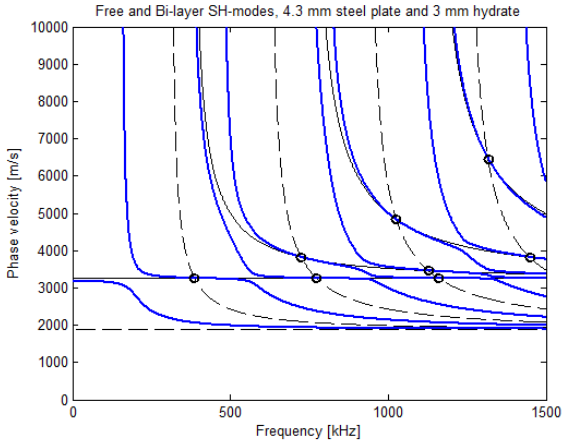


b)

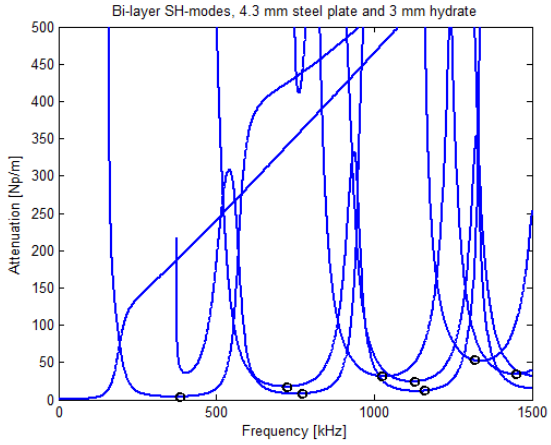


**Figure 7 a) 4.3 mm Steel plate in vacuum (solid black lines) and 3 mm $CH_4$ Hydrate free in vacuum (dashed lines). Black circles indicate "Free points". Steel-Hydrate bi-layer overlaid (blue lines). b) Attenuation of bi-layer modes with free points.**

In this section, it has been shown that bi-layer modes appearing from a hydrate deposit layer on a steel wall have some characteristic points which can be found by simple formulas and therefore be related to the layer thickness (though strictly only valid for plate modes). These points can be associated with frequencies of mode jumping and modes' attenuation minima.
The mode jumping is observed to result in a transition region of increased attenuation between two modes. It is however, not yet clear how strongly each mode is excited, and therefore how significant their attenuation is to the energy transfer over a given distance.

In Figure 8a the computed excitability functions of eq. 3, are compared with Rose's expression (eq. 4). A factor $4\pi$ difference was found between the results. This is not of concern here since it is the relative amplitudes that are sought.

a)

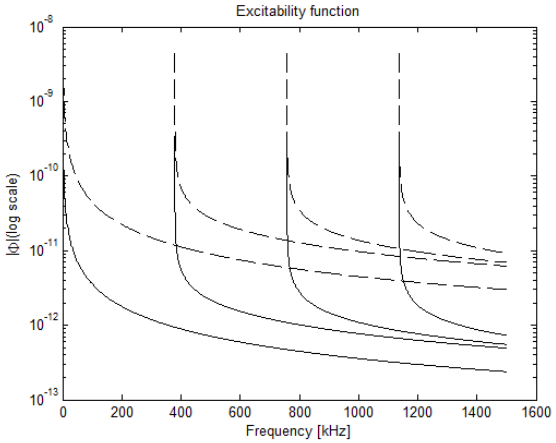


b)

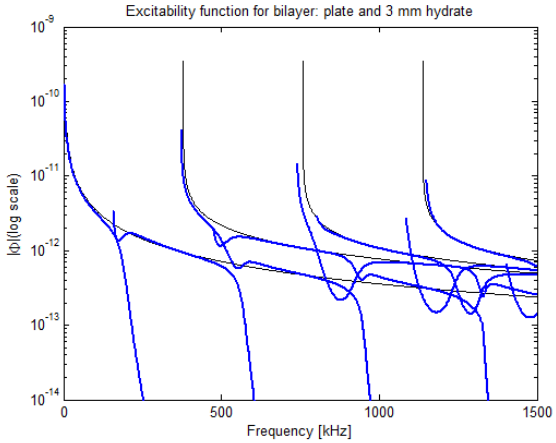


**Figure 8 Excitability functions for a 4.3 mm steel plate with traction surface source field normal to the direction of propagation (SH modes). a) Analytical expression from Rose [] (dashed lines), calculations using Modest (solid lines). b) Excitability of steel-hydrate bi-layer modes (blue lines) overlaid single steel layer excitability functions (black lines).**

Excitability functions for the 4.3 mm steel - 3 mm hydrate bi-layer are shown with blue lines in Figure 8b overlaying the excitability functions of the steel plate in vacuum. It is observed that the modes introduced by the hydrate layer start off with high values of excitability, while mode jumping can be associated with decreased excitability.

The modes are now propagated 0.5 m along the plate while taking attenuation into account, see Figure 9a. Comparing this figure with Figure 8b, it is found that the high amplitudes of the modes near cut-off are efficiently reduced by the high attenuation in that frequency range. Figure 9b shows a close up of the same frequency range as in the attenuation curves in Figure 6b. The same colour outlining near the rigid points is also used to follow the modes near the rigid points. The scale on amplitude axis in Figure 9b is logarithmic. Summing the contributions from the different modes will therefore nearly produce the envelope of the curves. It can be seen that this amplitude characteristic follow one that could be expected by simply following the path of lowest attenuation in Figure 6b. This means that the rigid and free points discussed above can be used to relate attenuation minima and maxima to the thickness of the deposit.

a)

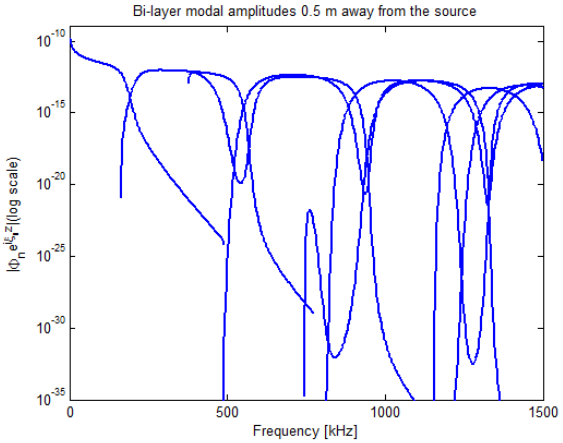


b)

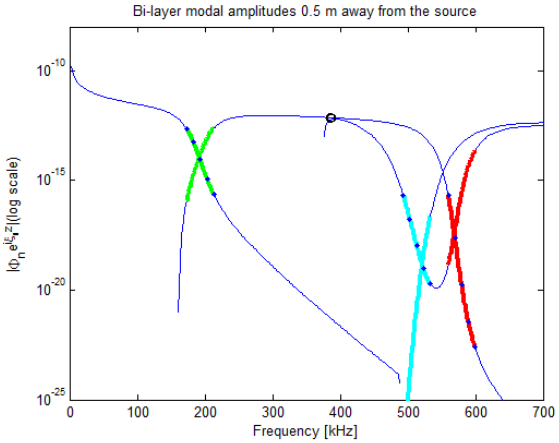


**Figure 9 Bi-layer simulation: 4.3 mm steel plate with 3 mm hydrate deposit. Modal amplitudes 0.5 m from the source where excitability and attenuation are accounted for. b) 40 kHz frequency band around rigid points outlined as in Figure 6. Black circle: Free point (m=1, n=0 in eq. 7)**

## 4 Experimental setup

Measurements were made on a 2" schedule 80 stainless steel pipe section (with an inner diameter of 490 mm) measuring 750 mm between the flanges. Plane surfaces were machined near each flange for transducer mounting. The diameter between the two transducer positions was cut on a lathe to fluctuate with the centre of the plane surfaces. The resulting wall thickness in the sensing area was 4.3 mm. Shear polarized 18x3x1 mm (LWD) pz27 piezo-electric elements from Ferroperm where glued to the machined surfaces of the pipe broadside the axial direction, 503 mm apart (one element near each flange). The elements and the area behind the elements were damped with a mix of araldite and wolfram powder. The pipe section between the elements was also damped to suppress helical waves. Most of the pipe section between the elements was damped using rubber paint. Only a direct path, a sensing area about 5 cm wide, was left undamped.

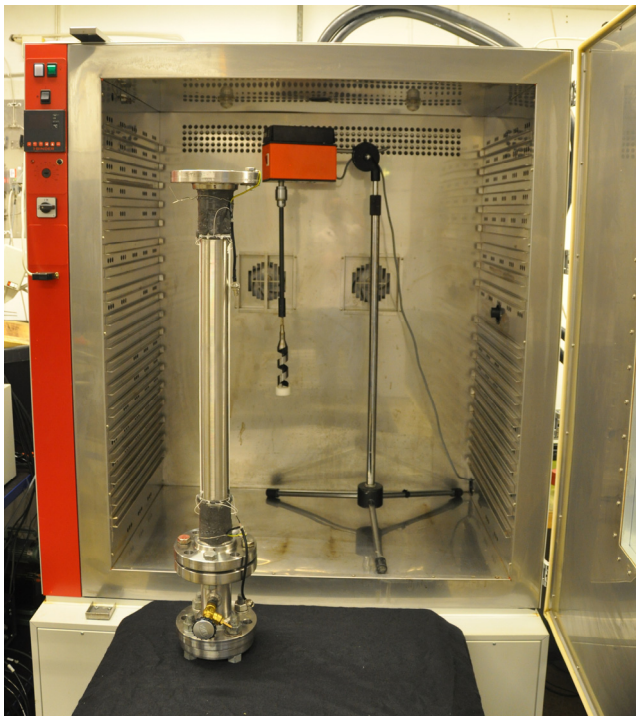

**Figure 10 Spool with transducer elements glued on used in experiments. Climate chamber and rotor with 30 mm drill bit used for stirring are shown in the back.**

One element was used as a sender, the other one as a receiver. A signal generator (NI-PXI 5421) was used for signal excitation and a KrohneHite filter Model 3940 was used on the receiver side before digitization in a NI-PXI 5122 digitizer.

The pipe was placed under a stirrer and put in a climate chamber. Five PT100 elements were used for temperature measurements inside the pipe 12, 24, 44, 60 and 85 cm from the top flange. One temperature probe was put outside the pipe in the chamber.

The multimodal dispersive signal attenuation was measured by comparing the signal energy content (the autocorrelation peak) with the signal energy content of a reference measurement (made on an empty pipe). The excitation signals were band limited sinusoidals with centre frequencies from 100 kHz to 1500 kHz, in 12.5 kHz steps. A 100 kHz bandwidth Hann window was used to band limit the signals.

A stirrer was used in the hydrate experiments and both stirrer and spool was put in a climate chamber, see Figure 10.

The hydrate experiments where made using a mixture of cyclopentane with 1 molar % Span 80 (emulsifier), distilled water and for some experiments, salt (NaCl). The cyclopentane referred to in the following given weight concentrations, is mixed with this emulsifier. cyclopentane was chosen since it produces sII hydrate structures at atmospheric pressure [18]. The climate chamber was set to 2 ºC in these experiments. Continuous mixing of the fluids was necessary and done by a 30 mm drill bit mounted on a rotor rotating at 400 rpm. Four to

six grams of ice was used to seed the cooled mixture to start the hydrate generation. The times of the seeding can be seen as a spike from the chamber temperature probe in Figures 13 to 15 below. Different concentrations of cyclopentane were tested as described in the description of each figure.

# 5 Results

## 5.1 Acoustical measurements of ice growth

Measurements were made every 90 seconds with distilled water in the pipe without stirring and the chamber temperature was set to -5 ºC.

a)

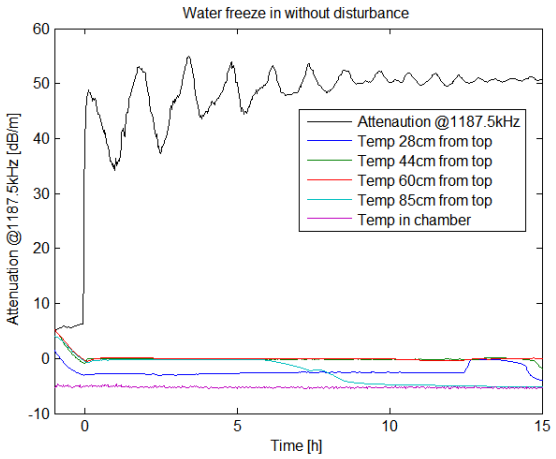


b)

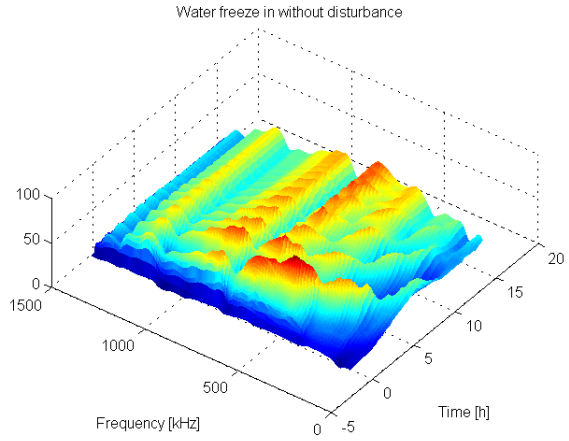


**Figure 11 Measurement of water freeze in. a) Attenuation at 1187.5 kHz (centre frequency) and temperature in chamber and inside pipe (see legend). b) Attenuation in dB/m ref. measurement in air as function of time and frequency.**

Figure 11a shows measured attenuation (in black) at 1187.5 kHz as function of time along with the temperature measurements (scale is degrees C for temperature measurements). In Figure 11b, attenuation (in dB/m relative to air measurement) is shown as function of time and frequency.

Figure 12a shows a top view of simulated attenuation for an increasing ice layer on 4.3 mm thick plate. The processing is done to match the case of the measurements. The calculations involve calculating: modal solutions, mode shapes, excitability functions, transfer functions, transferred signal (band limited excitation) and finally attenuation … for deposit layer thicknesses in the range 0-4 mm in steps of 0.1 mm. Overlaid the figure, are the rigid (∗) and free (o) points calculated with equations 6 and 7 for $n$=0.

Figure 12b shows a top view of Figure 11b. Here linear growth has been assumed and the rate of growth (here 0.7 mm/h) adjusted to best fit the rigid points for $m$=1 and $n$=0. Note that the other points follow from this parameter setting.

a)

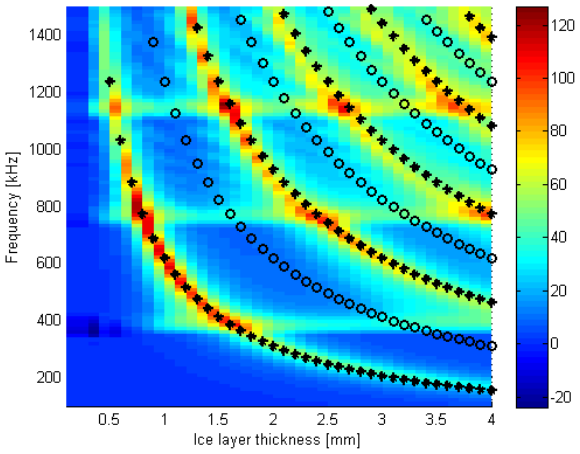


b)

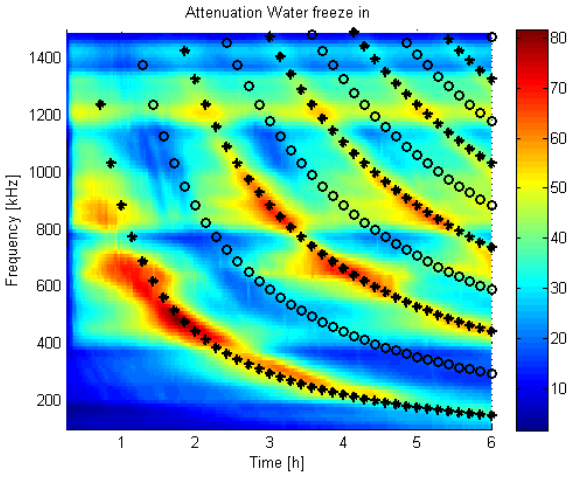


**Figure 12 Attenuation (in dB/m) on the colour scale with rigid and free points superimposed (ascetics and circles respectively). a) Simulations for a 4.3 mm steel plate with increasing ice layer thickness. b) Measurements (top view of Figure 11). Rigid and free points fitted by assuming linear growth of 0.7 mm/h.**

### 5.2 Acoustical measurements of hydrate formation

In Figure 13 the results of a run with 80% cyclopentane and 20% water is shown. The black curve shows the measured attenuation while the remaining cures show the different temperature measurements as described above. The picture is taken looking into the pipe from the top after the experiment when the pipe has been drained for liquid content. The chamber temperature was set to 2 ºC.

Figure 14 shows the results of a run where salt has been added to the solution (to obtain a water salinity of about 35‰). The fluid changed character quite dramatically when adding this salt. It had a higher tendency of separating and after emptying the pipe, the hydrates were observed to have grown on the drill bit (see Figure 15) and in the bottom of the pipe, but not on the pipe wall in the sensing area.

A pump circulating the fluid via an external hose was introduced for better mixing. Running the same fluid as above the hydrate now deposited on the wall (see picture in Figure 16b). Figure 16a shows the measured attenuation of this experiment.

Figure 17 and Figure 18 show the results of running a 20/80 cyclopentane/water mixture without salt. With this water concentration nearly all of the fluid could be frozen into hydrates. Figure 17 shows a “complete” cycle where the hydrates are formed (indicated by the first temperature increase), then the growth has stopped (and the temperature falls back towards the ambient temperature), and finally, the chamber was set to 10 degrees C and dissociation begun. In Figure 18, the results are shown from an experiment that was stopped 20 minutes after the first hydrate formation was detected. The pipe was drained and a picture of the resulting deposit is shown in Figure 18b.

Figure 19 show the results of running a 20/80 cyclopentane/water mixture with salt added to obtain a water salinity of about 35‰. Also this mixture went through dramatic changes as the salt was added. The fluid became jelly with distributed ice-like particles.

a)

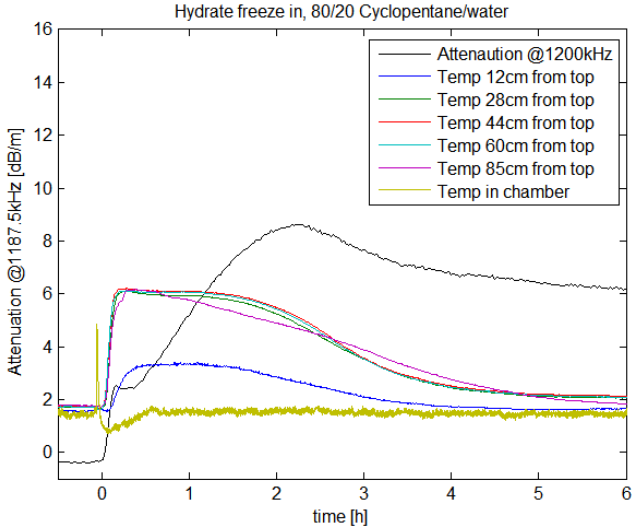


b)

**Figure 13 Hydrate experiment running 80% cyclopentane and 20% water. a) Measured attenuation and temperature. b) Picture looking into the pipe after draining excess fluid after the experiment.**

a)

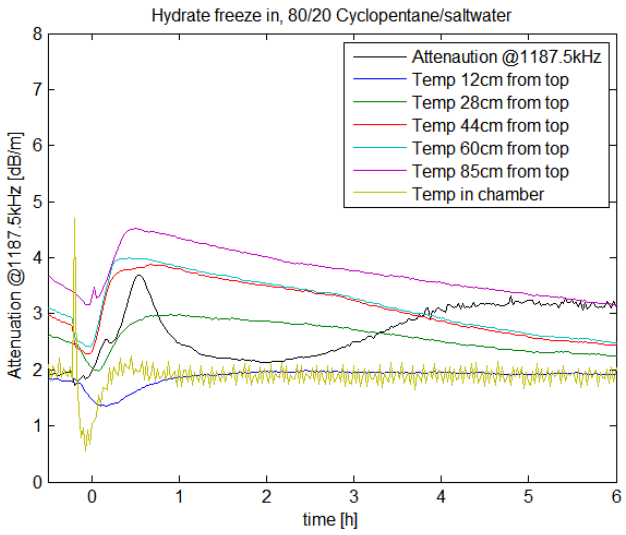


b)

**Figure 14 Hydrate experiment running 80% cyclopentane and 20% water with a salinity of 35‰. a) Measured attenuation and temperature. b) Picture looking into the pipe after draining excess fluid after the experiment.**

**Figure 15 Hydrate growth on drill bit (used for stirring) when salt (35‰ of water mass) was added to the solution of 80 % cyclopentane (by weight) and 20% water.**

a)

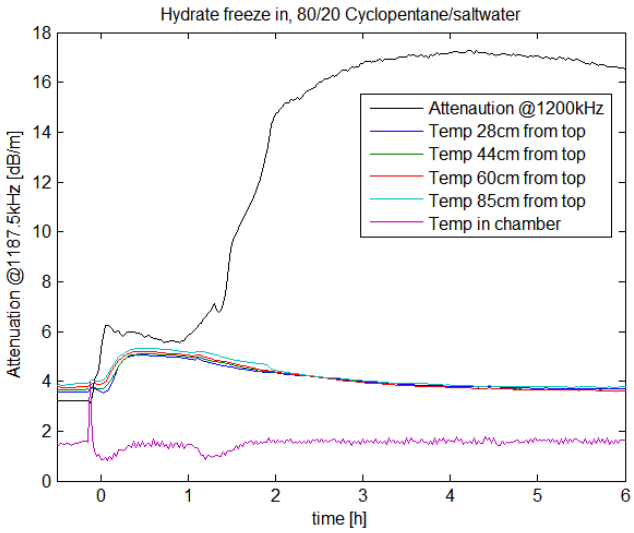


b)

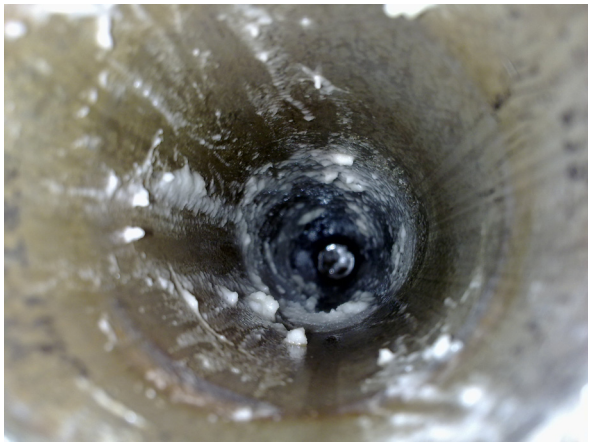

**Figure 16 Hydrate experiment running 80% cyclopentane and 20% water with a salinity of 35‰. The fluid was circulated and fed to the top with a pump outside the pipe. a) Measured attenuation and temperature. b) Picture looking into the pipe after draining excess fluid after the experiment.**

a)

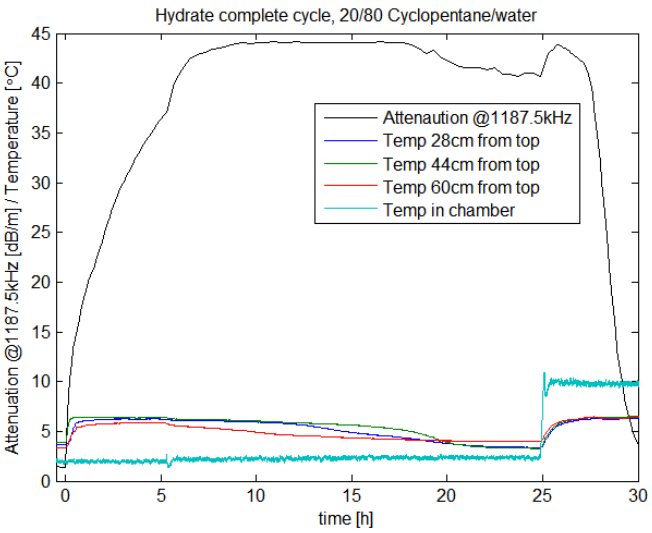


b)

**Figure 17 Hydrate experiment running 20% cyclopentane and 80% water. a) Measured attenuation and temperature. b) Drill bit covered with hydrates. The hydrates froze solid in this experiment.**

a)

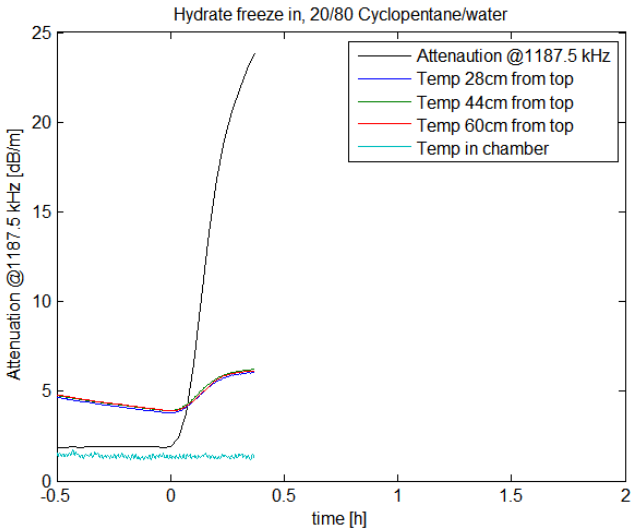


b)

**Figure 18 Hydrate experiment running 20% cyclopentane and 80% water. Experiment stopped 20 minutes after onset detection. a) Measured attenuation and temperature. b) Picture looking into the pipe after draining excess fluid after the experiment.**

a)

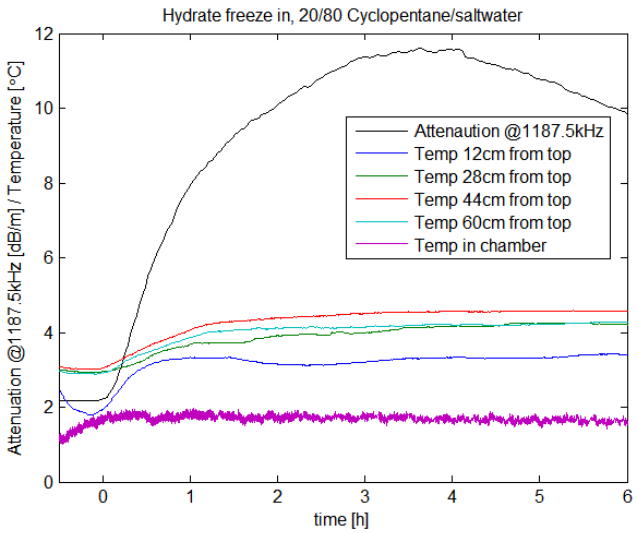


b)

**Figure 19 Hydrate experiment running 20% cyclopentane and 80% water with a salinity of 35‰. a) Measured attenuation and temperature. b) Picture looking into the pipe after extracting the drill bit. The solution became jelly with distributed solid particles.**

## 6 Discussion

Results from experiments with water and four different hydrate forming mixtures have been presented. The appearances of the hydrates formed were remarkably different for the different solutions. Still, an early detection of the onset was seen in all cases when compared with the times of temperature increase inside the pipe.

The detection was made by an increase in attenuation. The thickness of the deposit at the time of the first detection could not be obtained with this setup. The time of detection (with measurements taken every 90 seconds) was however found to correspond with the time of increase for the temperature probes (with measurement taken every 10 seconds).

Water showed, as the only solution, a characteristic oscillation in measured attenuation over time as it froze. It is believed that these oscillations where caused by the ice layer growing on the wall. Simulations have shown that the modes of a bi-layer introduce attenuation maxima and minima in the multimodal transduction. By analysing some properties of the bi-layer modes, an approximation of the relation between the frequency dependent attenuation maxima (and minima), and the thickness of the deposit layer was proposed: The attenuation maxima where related to the "rigid points" associated with the bi-layer (eq. 6 with $n$=0), while the attenuation minima where associated with the "free points" (eq. 7 with $n$=0). Adjusting only the growth rate (assumed constant) both maxima and minima where well described by the rigid and free points, see Figure 12b.

A stirrer had to be used in the hydrate experiments. This stirring can have resulted in a less uniform layer formation which may explain the lack of oscillations in the hydrate measurements. It is tempting to associate the level of attenuation with the amount of hydrates formed. This is probably also to a certain extent the case. But, as the water experiment has

shown, attenuation may fall off even as the layer grows. In addition, in the experiment of Figure 17, the attenuation is seen to fall off as the solid plug is developed. Furthermore, the attenuation increased as the "heat" was turned on. One explanation to this could be temperature dependency in the shear impedance of the hydrate with effects as discussed in section 3.2.

## 7 Conclusions

Using torsional modes, deposits can be detected with little disturbance from fluid flow.

Attenuation of multimode dispersive signals can be measured by looking at the energy content of the signal.

Attenuation is the best candidate for irregular or highly absorbing layers.

Layer thickness can be measured in the special cases where the deposit layer also makes a waveguide.

The time of onset detection was comparable with results from temperature measurements made inside the pipe.

## 8 Acknowledgements

The work presented here has been done as part of a PhD fellowship of the 1st author (2008-2011), under a 4-year strategic institute programme (SIP), "Multimodal flow assurance metering station (MuFAMES)" (2006-2009), which is carried out in a cooperation between Christian Michelsen Research AS, the University of Bergen (UoB) / Dept. of Physics and Technology, and Statoil ASA. The SIP is supported by the Research Council of Norway (NFR).

# 9 References


[1] E. D. Sloan and C. A. Koh, Clathrate Hydrates of Natural Gases, 2007.

[2] J. L. Rose, "A Baseline and Vision of Ultrasonic Guided Wave Inspection Potential", Journal of Pressure Vessel Technology 124, nr. 3 (2002): 273-282.

[3] T. R. Hay and J. L, Rose, "Fouling detection in the food industry using ultrasonic guided waves", Food Control 14, 7 (October 2003): 481-488.

[4] J. O. Kim and H. H. Bau. "Instrument for simultaneous measurement of density and viscosity." Review of Scientific Instruments 60, no. 6 (1989): 1111-1115.

[5] R. A. Kippersund, P. Lunde, K-E. Frøysa, 2010, "Measurement of fluid viscosity in pipes using multimode ultrasonic guided wave attenuation", Proc. of Baltic-Nordic Acoustic Meeting (BNAM), Bergen, May 2010.

[6] P.D. Wilcox, M.J.S. Lowe, og P. Cawley, "Mode and Transducer Selection for Long Range Lamb Wave Inspection2, Journal of Intelligent Materials Systems and Structures 12, nr. 8 (2001): 553-565.

[7] L. Knopoff. "A matrix method for elastic wave problems." Bulletin of the Seismological Society of America 54, no. 1 (1964): 431-438.

[8] B. Pavlakovic, M. J. S. Lowe, D. Alleyne and P. Cawley. "Disperse: a general purpose program for creating dispersion curves." In Review of Progress in Quantitative Nondestructive Evaluation: Proceedings of the Twenty-Third Symposium Held in Brunswick, Maine, July 28-August 2, 1996, (1997).

[9] J. L. Rose, Ultrasonic Waves in Solid Media (Cambridge University Press, 2004).

[10] B. A. Auld, Acoustic Fields and Waves in Solids, Vol. 2, 2. edition. (Krieger Pub Co, 1990).

[11] L. Duquenne et. al. , "Transient modelling of Lamb waves generated in viscoelastic materials by surface bonded piezoelectric transducers", The Journal of the Acoustical Society of America 116, nr. 1 (July 2004): 133-141.

[12] M.J.S. Lowe og F. Simonetti, with J. Ma, "Measurement of the properties of fluids inside pipes using guided longitudinal waves", Ultrasonics, Ferroelectrics and Frequency Control, IEEE Transactions on 54, nr. 3 (2007): 647-658.

[13] William F. Waite et. al., "Laboratory Measurements of Compressional and Shear Wave Speeds through Methane Hydrate", Annals of the New York Academy of Sciences 912, nr. 1 (2006): 1003-1010.

[14] M. G. Silk og K. F. Bainton, "The Propagation in Metal Tubing of Ultrasonics Wave Modes Equivalent to Lamb Waves", Ultrasonics 71, nr. 1 (1979): 11–19.

[15] B. N. Pavlakovic, "Leaky guided ultrasonic waves in NDT," Ph.D. thesis, University of London, Imperial College of Science, technology and medicine, 1998

[16] R. A. Kippersund, P. Lunde and K-E Frøysa. "Deposit detection using plate waves", Proceedings of the 32th Scandinavian Symposium on Physical Acoustics, Geilo 8 – 11 February, 2011.

[17] F. Simonetti, "Sound propagation in lossless waveguides coated with attenuative materials", Ph.D. thesis, University of London, Imperial College of Science, technology and medicine, 2004.

[18] M. Nakajima, R. Ohmura, og Y. H. Mori, "Clathrate Hydrate Formation from Cyclopentane-in-Water Emulsions", Industrial & Engineering Chemistry Research 47, nr. 22 (november 19, 2008): 8933-8939.